

Showcasing research from Professor Hexin Xie's laboratory, School of Pharmacy, East China University of Science and Technology (ECUST), Shanghai, China.

A self-immobilizing near-infrared fluorogenic probe for sensitive imaging of extracellular enzyme activity *in vivo*

A research team led by Professor Xie integrates quinone methide and fluorescent enzyme substrate to develop a self-immobilizing near-infrared fluorogenic probe for the visualization of extracellular enzyme activity in living animals. This imaging reagent covalently traps around target enzymes and massively enhances fluorescence intensity at 710 nm simultaneously upon selective activation by the enzyme. Compared to common fluorogenic sensors, this probe significantly prolongs the retention of the fluorescence signal at the detection target and thus improves sensitivity at highly dynamic *in vivo* systems.

As featured in:



See Hexin Xie *et al.*,
Chem. Sci., 2020, 11, 5889.

Cite this: *Chem. Sci.*, 2020, 11, 5889 All publication charges for this article have been paid for by the Royal Society of Chemistry

Received 2nd March 2020

Accepted 11th May 2020

DOI: 10.1039/d0sc01273d

rsc.li/chemical-science

A self-immobilizing near-infrared fluorogenic probe for sensitive imaging of extracellular enzyme activity *in vivo*†

Yuyao Li,^a Heng Song,^a Chenghong Xue,^a Zhijun Fang,^a Liqin Xiong ^b and Hexin Xie ^{*a}

Reported herein is a self-immobilizing near-infrared fluorogenic probe that can be used to image extracellular enzyme activity *in vivo*. Using a fluorophore as a quinone methide precursor, this probe covalently anchors at sites of activation and greatly enhances the fluorescence intensity at 710 nm upon enzymatic stimulus, significantly boosting detection sensitivity in a highly dynamic *in vivo* system.

Introduction

Fluorescence imaging reagents have emerged as powerful tools in biological studies and clinical diagnosis owing to their high operational simplicity, spatial and temporal resolution, and non-invasiveness.¹ In particular, activity-based fluorogenic probes with absorption and emission in the near-infrared (NIR) region, which reduce auto-fluorescence and allow visualization of a signal in deeper tissues, are preferential in the imaging of enzyme activities *in vivo*.² However, an *in vivo* system is an open and highly dynamic physiological environment. Most current small molecule-based fluorescent probes, in spite of their massive increase in fluorescence intensity after enzymatic activation, are inevitably limited by the rapid diffusion of activated fluorophores from activation sites and lead to a decreased signal-to-background ratio (SBR) in the *in vivo* imaging of the activity of enzymes, especially extracellular enzymes.³

To address this challenge, activated fluorophores, rather than intact fluorescent probes, are required to have prolonged retention at the site of interest. Rao and colleagues developed a target enabled *in situ* ligand aggregation (TESLA) strategy, in which small molecules assemble non-covalently into nanostructures to confer high retention of imaging reagents after enzymatic stimuli.⁴ Xu's group, on the basis of a Phe–Phe dipeptide-based hydrogelator, established an enzyme-triggered molecular self-assembly approach for the detection of enzyme activity in live cells.⁵ This approach was further explored in the

in vivo imaging of enzyme activity by the Liang⁶ and Wang⁷ groups.

Quinone methides (QMs)⁸ are transient molecules with exceptionally high electrophilicity. Taking advantage of this property, QM-based probes have been exploited to report enzyme activities *in vivo*.⁹ These imaging reagents, upon enzymatic activation, generate highly reactive QMs to react with nucleophiles from the exterior of the target enzyme or proteins nearby, and thus elicit the retention of fluorophores, allowing visualization of enzyme activities in dynamic environments. Nevertheless, these “always-on” probes lack the ability to amplify the fluorescence signal after activation and thus compromise detection sensitivity. Incorporating a fluorescent probe and the chemistry of QM, Withers and co-workers developed a fluorogenic and self-immobilizing probe to image the β -glucuronidase activity in an *Arabidopsis thaliana* plant line.¹⁰ While this approach has been further explored in the fluorescent probes of various enzymes and promising results have been reported in cell-based imaging,¹¹ visualization of enzymatic transformations in live animals with these reagents has not been realized, mainly due to short absorption and emission wavelengths. The key characteristics of ideal fluorescent probes for *in vivo* imaging include a high fluorescence turn-on ratio, brightness, and bio-stability, as well as absorption and emission wavelengths in the NIR region and high retention of activated fluorophore. Herein, we report a self-immobilizing and NIR fluorogenic probe, which shows significantly improved detection sensitivity in the imaging of extracellular enzyme activity in living mice.

Alkaline phosphatase (ALP) is a type of extracellular plasma membrane-anchored hydrolyse, facilitating the dephosphorylation process for a variety of molecules.¹² Elevated activity of ALP is closely related to a range of diseases; this enzyme has been considered as an important biomarker for clinical diagnosis. To reveal the ALP activity in a physiological environment, a number of fluorescent probes have been developed.¹³ While

^aState Key Laboratory of Bioreactor Engineering, Shanghai Key Laboratory of New Drug Design, School of Pharmacy, East China University of Science and Technology, Shanghai 200237, P. R. China. E-mail: xiehixin@ecust.edu.cn

^bShanghai Med-X Engineering Center for Medical Equipment and Technology, School of Biomedical Engineering, Shanghai Jiao Tong University, Shanghai 200030, P. R. China

† Electronic supplementary information (ESI) available. See DOI: 10.1039/d0sc01273d



these reagents exhibit an excellent fluorescent turn-on ratio in solution-based tests, the *in vivo* imaging of ALP activity with these probes is still somewhat limited, which is likely because of the fast diffusion of activated fluorophores in dynamic environments. Very recently, Ye and colleagues combined a regular near-infrared fluorogenic probe with the Phe-Phe dipeptide-based self-assembly strategy to develop an intriguing NIR fluorogenic and self-assembling sensor for the *in vivo* imaging of ALP activity.¹⁴ In this study, we used ALP as a model enzyme to investigate a QM-based self-immobilizing and NIR fluorogenic probe.

Results and discussion

Design of the self-immobilizing NIR probe

Fig. 1 shows the design of a self-immobilizing NIR probe, in which an optically tunable NIR dye, HD¹⁵ with a zwitterion is used as an activatable fluorophore. This type of NIR dye has been widely explored in a range of fluorogenic probes of enzymes,¹⁶ including ALP.^{13a-c,14} To convert HD dye itself into a QM precursor, a monofluoromethyl group is introduced to the phosphate-caged NIR fluorophore. We envisaged ALP-promoted removal of phosphate leads to the leaving of a fluoro group and the HD NIR fluorophore thus becomes a highly reactive QM, which then reacts with nucleophilic proteins to covalently bond with the site of interest and resume NIR fluorescence. Recent studies¹⁷ have indicated that hydroxyl group-containing hemicyanine dyes are fluorescently sensitive to their cellular environment, including polarity, viscosity, and pH. However, these factors may affect this self-immobilizing ALP probe less as the target enzyme is located in the outer membrane of cells and the majority of activated fluorophores may presumably anchor covalently at the proteins of the outer surface of cells. However, to our surprise, monofluoromethylated ALPIN-2 is highly unstable in phosphate buffered saline (PBS, pH 7.4), resulting in it mostly hydrolyzing to ALPIN-OH in 0.5 h at room temperature (Fig. S1†), despite the monofluoromethyl group having been widely adopted in QM precursors.^{11a,c,f-h}

We thus turned our attention to the use of a more stable QM precursor. A probe with ethyl carbamate as a leaving group (ALPIN-3) did prove to be more stable in PBS. However, incubation of this molecule with ALP failed to elicit any enhancement in fluorescence intensity (Fig. S2a†). Further analysis of this sample using high-performance liquid chromatography (HPLC) confirmed ALP to be ineffective in the hydrolysis of ALPIN-3 (Fig. S2c†), whereas this enzyme is highly efficient in terms of the hydrolysis of its leaving group-free counterpart, ALPIN-1 (Fig. S2b†). We envisaged that the difference in enzyme kinetics comes from the steric hindrance of ethyl carbamate. With this in mind, we then introduced a benzyl ether linker between fluorophore and an enzymatic recognition moiety to minimize the steric impact on the enzyme. The carbamate-bearing ALPIN-5 and leaving group-free ALPIN-4 (as control) were synthesized, as outlined in Fig. S3.†

Optical characterization of the self-immobilizing NIR probe

With this pair of probes in hand, we first studied their absorption spectra before and after incubation with a small amount of ALP. As shown in Fig. 2a and b, ALPIN-4 and ALPIN-5 share very similar absorption spectra before and after enzymatic activation. Fluorescence spectra of these molecules with or without incubation with ALP were also recorded and a similar trend in these reagents was observed, but the maximum fluorescence intensity of the activated ALPIN-5 was slightly lower. We surmised this may be due to the lack of sufficient nucleophilic proteins in this test; where less nucleophilic water served as the major nucleophile. However, a cellular environment is much more complicated compared to a simple test tube-based solution. To mimic the nucleophilic protein-containing cellular environment, we applied β -mercaptoethanol (β -ME) as an extra nucleophile. As expected, the addition of β -ME indeed further enhanced the fluorescence of ALP-incubated ALPIN-5 (Fig. 2d). As a control, the incubation of ALPIN-5 with β -ME in the absence of ALP resulted in no change in the fluorescence intensity, indicating that this imaging reagent is compatible with thiols in the cellular environment. To further test the

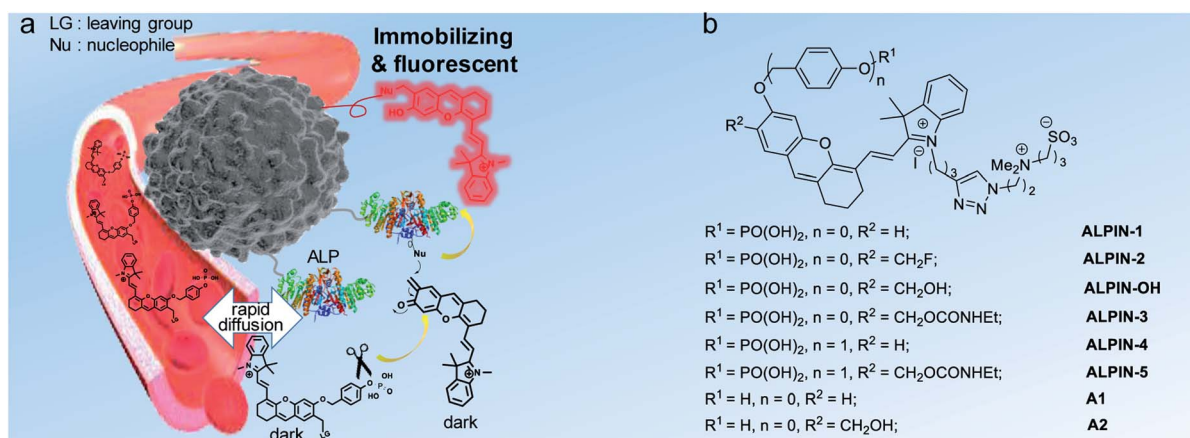


Fig. 1 (a) Design of a self-immobilizing and NIR fluorogenic probe for the *in vivo* imaging of extracellular enzyme activity. (b) Chemical structures of the NIR probes and fluorophores used in this study.



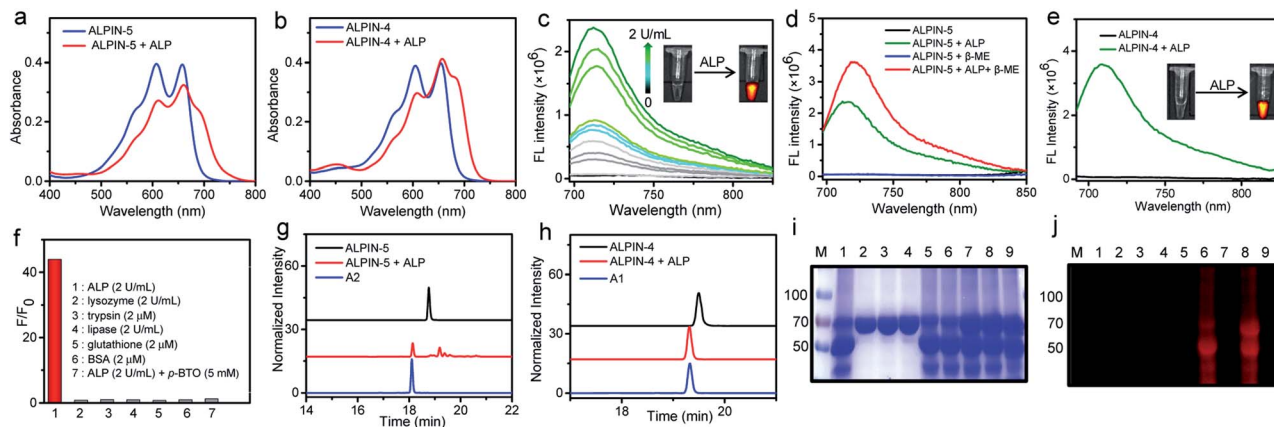


Fig. 2 (a) UV-Vis absorption spectra of ALPIN-5 (10 μM) or ALPIN-4 (10 μM) (b) in PBS (pH 7.4) before and after incubation with ALP (2 U mL^{-1}) at 37 $^{\circ}\text{C}$ for 30 min. (c) Fluorescence spectra of ALPIN-5 (10 μM) upon incubation with a serial of concentrations of ALP (0–2 U mL^{-1} , 37 $^{\circ}\text{C}$) for 30 min. (d) Fluorescence spectra of ALPIN-5 (10 μM) before and after incubation with ALP (2 U mL^{-1}) in the presence or absence of β -mercaptoethanol (140 mM) in PBS at 37 $^{\circ}\text{C}$ for 30 min. (e) Fluorescence spectra of ALPIN-4 (10 μM) before and after incubation with ALP (2 U mL^{-1}) in PBS at 37 $^{\circ}\text{C}$ for 30 min. (f) Fluorescence response of ALPIN-5 (10 μM) to various analytes in PBS. $\lambda_{\text{ex}}/\lambda_{\text{em}} = 687/714 \text{ nm}$ (g) HPLC traces of ALPIN-5 (10 μM) or ALPIN-4 (h) before and after incubation with ALP (2 U mL^{-1}) at 37 $^{\circ}\text{C}$ for 30 min. (i) Coomassie blue staining and fluorescence imaging (j) of SDS-PAGE gel. The indicated protein was incubated with or without probes in PBS at 37 $^{\circ}\text{C}$ for 2 h. M: protein marker; 1: ALP; 2: BSA; 3: BSA + ALPIN-4; 4: BSA + ALPIN-5; 5: ALP + ALPIN-4; 6: ALP + ALPIN-5; 7: ALP + BSA + ALPIN-4; 8: ALP + BSA + ALPIN-5; 9: ALP + BSA + *p*-BTO + ALPIN-5. *p*-BTO: (–)-*p*-bromotetramisole oxalate, an ALP inhibitor; $\lambda_{\text{ex}}/\lambda_{\text{em}} = 685/720 \text{ nm}$.

specificity of ALPIN-5, we incubated this reagent with a number of biological analytes, including lysozyme, trypsin, lipase, glutathione, and bovine serum albumin (BSA), as well as ALP (Fig. 2f). It turned out that only ALP led to a notable enhancement in fluorescence; the others showed no impact on the fluorescence of this probe. Furthermore, the activation of NIR fluorescence by ALP was greatly suppressed by the addition of (–)-*p*-bromotetramisole oxalate (*p*-BTO), an ALP inhibitor.

Additionally, we employed HPLC to analyze these enzyme-incubated samples (Fig. 2g and h). Unlike ALPIN-4, which produced only free fluorophore A1, the ALP-treated ALPIN-5 yielded a mixture of fluorophore-containing compounds, including fluorophore A2. These molecules likely resulted from nucleophilic addition to the transient QM intermediate by a variety of nucleophiles, including water.

To validate whether ALPIN-5 is capable of covalently labeling proteins after enzymatic activation, we incubated this molecule with ALP alone or a mixture of ALP and BSA and then analyzed their labeling using in-gel fluorescence imaging. As shown in Fig. 2j, ALPIN-5 induced strong NIR fluorescence signals for all of these proteins, while the addition of ALP inhibitor (*p*-BTO) significantly reduced the fluorescence in the gel. Moreover, incubation of ALPIN-5 and BSA in the absence of ALP resulted in non-fluorescence on the protein. These results demonstrate that ALPIN-5 is able to connect the target enzyme or nearby proteins covalently after selective enzymatic activation. Notably, the ability of ALPIN-5 to label both target enzyme and nearby nucleophilic proteins is advantageous for *in vivo* imaging as this allows more activated fluorophore to be retained around the site of activation, not limited by the number of nucleophilic residues from the target enzyme. In sharp contrast, the leaving group-free probe, ALPIN-4, was unable to produce any

fluorescence on the protein band of ALP or BSA, even with a high fluorescence turn-on ratio.

Imaging of ALP activity in live cells

Having demonstrated the covalent labeling of proteins with ALPIN-5, we then moved to cell-based imaging. Cytotoxicity of ALPIN-5 was first assessed using a standard MTT assay (Fig. S4†), which indicated that the viability of HeLa cells was unaffected by ALPIN-5 at up to 20 μM . We thus incubated ALP-overexpressing HeLa cells with ALPIN-5 and imaged them using a regular fluorescence microscope. Upon washing away any unbound fluorophore, we observed much more intense NIR fluorescence from the ALPIN-5-treated HeLa cells compared to the ALPIN-4-treated cells (Fig. 3a). Additionally, the incubation of ALPIN-5 with HeLa cells pre-treated with an ALP inhibitor, Na_3VO_4 , or ALP-negative HEK293 cells barely produced any NIR fluorescence.

To further compare the fluorescence of HeLa cells, we analyzed these probe-treated HeLa cells using flow cytometry (Fig. 3b) and the results were found to be consistent with the aforementioned cell images: self-immobilizing ALPIN-5 generates a more intense fluorescence signal on HeLa cells over ALPIN-4, even though these two reagents exhibit a comparable fluorescence response in aqueous solution (Fig. 2). These results indicate that the self-immobilizing fluorescent probe limits the diffusion of activated fluorophore and leads to a higher SBR and improved detection sensitivity.

After enzyme activation, ALPIN-5 is capable of enhancing fluorescence intensity and trapping covalently at or near the sites of activation, which makes it possible to visualize enzyme activity in cells without washing away the free fluorophore and thus allows real-time imaging. As expected, after incubation of



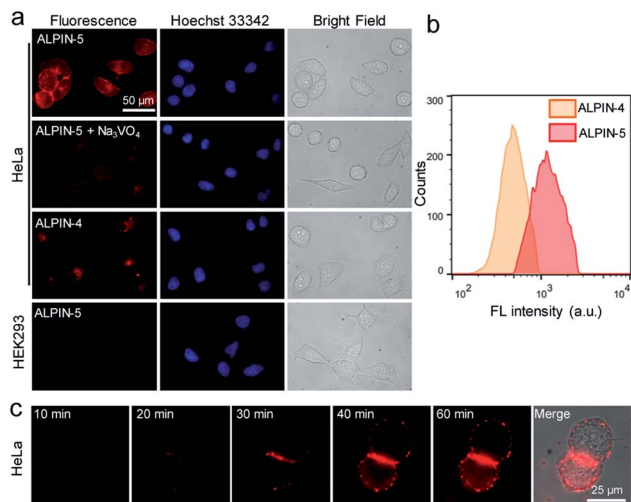


Fig. 3 (a) Fluorescence imaging of HeLa and HEK293 cells with the probes. ALPIN-5 or ALPIN-4 (10 μ M) was incubated at 37 $^{\circ}$ C for 1 h with the indicated cells, as well as cells pretreated with Na_3VO_4 (10 mM), an ALP inhibitor, for 20 min before incubation with the probe. (b) Flow cytometry of HeLa cells incubated with ALPIN-5 or ALPIN-4 (10 μ M). (c) Wash-free and real-time fluorescence imaging of HeLa cells incubated with ALPIN-5 (1 μ M). Fluorescence images were acquired using a Cy5.5 channel.

self-immobilizing ALPIN-5 with HeLa cells, we observed a constant increase in the NIR fluorescence on cells over 1 h (Fig. 3c). And the majority of the fluorescence signal appears to come from the surface of the HeLa cells, which is consistent with a previous report in which ALP was found to be mainly located in the plasma membrane of HeLa cells.¹⁸

Imaging of ALP activity in living mice

Prior to applying ALPIN-5 in live animals, we tested this compound, as well as ALPIN-4, on a tissue slice of a xenografted HeLa tumor in a mouse. Again, a much more intense fluorescence signal was detected from the ALPIN-5-treated sample compared to that of ALPIN-4, further confirming the superior fluorescent labeling ability of ALPIN-5 (Fig. 4a).

We next turned our attention to the imaging of ALP activity in living mice with ALPIN-5. To compare the retention of ALPIN-4 and ALPIN-5 in tumor, we intratumorally injected these molecules into mice with subcutaneously implanted HeLa tumors and monitored the fluorescence over time (Fig. 4 and S5[†]). For the ALPIN-4-treated mice, the fluorescence on tumor reached its maximum intensity at around 10 min post injection and then dropped rapidly. This is likely a result of two factors: (1) the enhancing of fluorescence by enzymatic activation; and (2) fast diffusion of the fluorophore from the tumor. Yet, the self-immobilizing ALPIN-5 delivered much more intense NIR fluorescence on the tumor and, more notably, lasted much longer. A substantial signal on tumor was detected even after 48 h post injection, indicating that the integration of QM with the fluorogenic probe significantly improves the retention of activated fluorophore in the tumor.

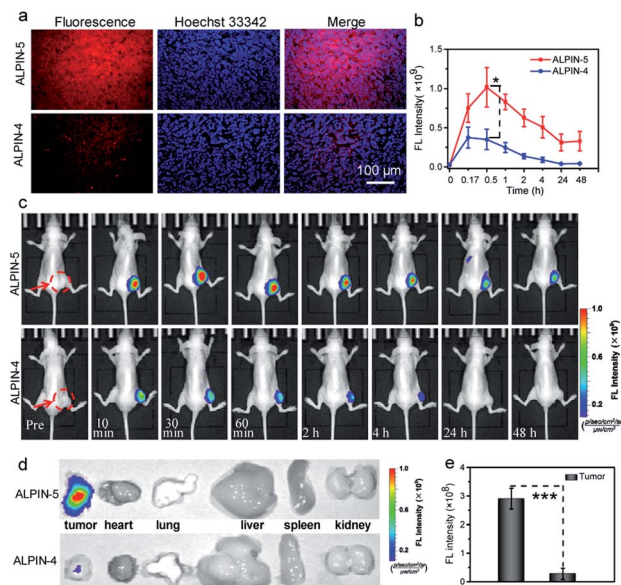


Fig. 4 (a) Fluorescence imaging of a tissue slice of a xenografted HeLa tumor in mice with ALPIN-5 or ALPIN-4. (b) Fluorescence intensity or representative fluorescence imaging (c) of ALP activity in HeLa tumor-bearing mice after i.t. injection of probes. (d) Fluorescence images of tumor and main organs at 48 h post injection. $\lambda_{\text{ex}}/\lambda_{\text{em}} = 660/710$ nm. (e) Quantitative fluorescence intensity of tumors in (d). Values are the mean \pm SD (* $P < 0.05$, *** $P < 0.001$, $n = 3$). The red arrows and circles indicate the tumor locations in the mice.

Encouraged by these results, we further investigated the accumulation of these probes in ALP-overexpressing-tumor. After injecting self-immobilizing ALPIN-5 into the tail vein of HeLa tumor-bearing mice, we were able to detect an intense fluorescence signal at the site of the tumor at 1 h post injection and the fluorescence intensity had further increased at 2 h after injection. Even 24 h after injection, an obvious fluorescence signal was still detectable in the region of the HeLa tumor. Intratumoral injection of the ALP inhibitor Na_3VO_4 before intravenous injection of ALPIN-5 reduced the intensity of the fluorescence signal at the tumor, suggesting that the observed fluorescence signal from the tumor site indeed resulted from the activity of ALP. As a control, the regular fluorogenic probe ALPIN-4 delivered much lower intensity of NIR fluorescence in the region of the tumor at 1 h post injection, and then the signal dropped rapidly to nearly background level (Fig. 5 and S6[†]). These results demonstrate that the use of self-immobilizing fluorogenic probe not only expands the time window of imaging enzyme activity, but also massively enhances detection sensitivity.

The *ex vivo* fluorescence images of normal organs along with the HeLa tumor collected at 2 h post injection were also recorded (Fig. 5c, d and S6b[†]). The trend in the fluorescence intensity was found to be consistent with the aforementioned *in vivo* results: the self-immobilizing probe ALPIN-5 generated the most intense NIR fluorescence on the tumor and pretreatment of the tumor with ALP inhibitor diminished the signal on the tumor, whereas ALPIN-4 resulted in much less intense fluorescence. The liver and kidney are known to have elevated ALP



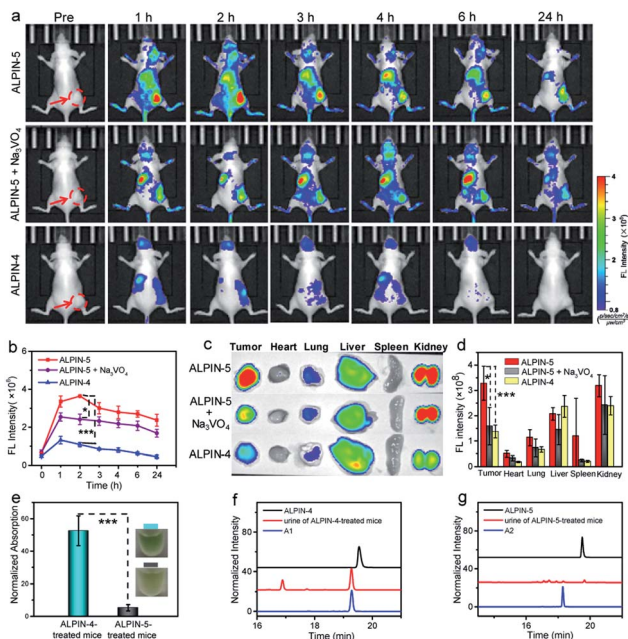


Fig. 5 (a) Representative fluorescence imaging or (b) fluorescence intensity of ALP activity in HeLa tumor-bearing mice after i.v. injection of the probes or together with i.t. injection of Na_3VO_4 (10 mM, 50 μL) before i.v. injection of ALPIN-5. (c) Fluorescence images of tumor and main organs at 2 h after i.v. injection of ALPIN-5, ALPIN-4, or ALPIN-5 together with i.t. injection of Na_3VO_4 . (d) Fluorescence intensity of organs and tumors in (c). $\lambda_{\text{ex}}/\lambda_{\text{em}} = 660/710$ nm. (e) Absorption (600 nm) of urine from probe-injected mice at 0.5 h post i.v. injection. (f) Representative HPLC traces of urine from ALPIN-4- or (g) ALPIN-5-treated mice 0.5 h post i.v. injection. Values are the mean \pm SD ($*P < 0.05$, $***P < 0.001$, $n = 3$). The red arrows and circles indicate the tumor locations in the mice.

activity^{12e} and we did observe considerable fluorescence from these organs in ALPIN-5-treated mice.

During the *in vivo* imaging of the enzyme activity, we accidentally noticed that the urine from treated mice was a bit bluer than that of the untreated mice. We thus collected urine from ALPIN-4- and ALPIN-5-treated mice at 0.5 h post injection. The urine from the ALPIN-4-treated mice looked obviously bluer than that of the ALPIN-5-treated mice (Fig. 5e). Analysis using HPLC confirmed there were NIR fluorophores in both samples while urine from the ALPIN-4-treated mice apparently contained much more dye than that of the ALPIN-5-treated mice (Fig. 5f and g). Moreover, from the HPLC trace of the ALPIN-4-leading sample, we detected two major components; one identified as free fluorophore A1 using UV-Vis spectrum and high-resolution mass spectrometry (HRMS) and the other determined to be glucuronidated A1 (A1G) in a similar manner (Fig. S7[†]).

Urine of the treated mice at different time points was also collected and analyzed by HPLC. As shown in Fig. S8[†], many more fluorophore-containing molecules were detected in the urine from the ALPIN-4-injected mouse compared to that from the ALPIN-5-treated mouse, particularly within 2 h post injection. These results suggest that self-immobilizing ALPIN-5 may have a much slower renal clearance rate in mice compared to

ALPIN-4, which is likely due to the immobilization of ALPIN-5 at the sites of activation, although other possibilities cannot be ruled out at the current stage.

Conclusions

In conclusion, we developed a novel self-immobilizing and NIR fluorogenic probe for the *in vivo* visualization of extracellular ALP activity. With an activatable NIR fluorophore itself as a quinone methide precursor, this imaging reagent massively enhances fluorescence intensity and covalently labels target enzymes or proteins nearby upon selective activation by the enzyme, limiting the rapid diffusion of activated fluorophore from sites of interest in a highly dynamic *in vivo* system. This self-immobilizing probe exhibits significantly improved sensitivity in the *in vitro* and, more notably, *in vivo* imaging of the activity of extracellular ALP compared to a regular fluorogenic reagent. This quinone methide-based self-immobilizing strategy may be applicable to other fluorescent enzyme substrates, facilitating the sensitive imaging of enzyme activities in living animals.

Conflicts of interest

There are no conflicts to declare.

Acknowledgements

All animal procedures were performed in accordance with the Guidelines for the Care and Use of Laboratory Animals of Shanghai Jiao Tong University and approved by the Animal Ethics Committee of Shanghai Jiao Tong University. This study was financially supported by the Recruitment Program for Young Professionals (H. X.), the Research Program of State Key Laboratory of Bioreactor Engineering (H. X.), the Fundamental Research Funds for the Central Universities (H. X.), NSFC-BRICS (81861148020, H. X.), and the NSFC (81974273, L. X.).

Notes and references

- (a) A. Razgulin, N. Ma and J. Rao, *Chem. Soc. Rev.*, 2011, **40**, 4186–4216; (b) J. Chan, S. C. Dodani and C. J. Chang, *Nat. Chem.*, 2012, **4**, 973–984; (c) R. Yan and D. Ye, *Sci. Bull.*, 2016, **61**, 1672–1679; (d) W. Chyan and R. T. Raines, *ACS Chem. Biol.*, 2018, **13**, 1810–1823; (e) H. W. Liu, L. Chen, C. Xu, Z. Li, H. Zhang, X. B. Zhang and W. Tan, *Chem. Soc. Rev.*, 2018, **47**, 7140–7180; (f) J. Zhang, X. Chai, X. P. He, H. J. Kim, J. Yoon and H. Tian, *Chem. Soc. Rev.*, 2019, **48**, 683–722.
- (a) Z. Guo, S. Park, J. Yoon and I. Shin, *Chem. Soc. Rev.*, 2014, **43**, 16–29; (b) S. A. Hilderbrand and R. Weissleder, *Curr. Opin. Chem. Biol.*, 2010, **14**, 71–79.
- I. Johnson, *Histochem. J.*, 1998, **30**, 123–140.
- (a) G. Liang, H. Ren and J. Rao, *Nat. Chem.*, 2010, **2**, 54–60; (b) B. Shen, J. Jeon, M. Palner, D. Ye, A. Shuhendler, F. T. Chin and J. Rao, *Angew. Chem., Int. Ed.*, 2013, **52**, 10511–10514; (c) D. Ye, A. J. Shuhendler, L. Cui, L. Tong, S. S. Tee,



- G. Tikhomirov, D. W. Felsher and J. Rao, *Nat. Chem.*, 2014, **6**, 519–526; (d) D. Ye, A. J. Shuhendler, P. Pandit, K. D. Brewer, S. S. Tee, L. Cui, G. Tikhomirov, B. Rutt and J. Rao, *Chem. Sci.*, 2014, **4**, 3845–3852.
- 5 (a) Z. Yang, G. Liang and B. Xu, *Acc. Chem. Res.*, 2008, **41**, 315–326; (b) Y. Gao, J. Shi, D. Yuan and B. Xu, *Nat. Commun.*, 2012, **3**, 1033; (c) J. Zhou, X. Du, C. Berciu, H. He, J. Shi, D. Nicastro and B. Xu, *Chem*, 2016, **1**, 246–263.
- 6 C. F. Wu, R. Zhang, W. Du, L. Cheng and G. L. Liang, *Nano Lett.*, 2018, **18**, 7749–7754.
- 7 D. Zhang, G. B. Qi, Y. X. Zhao, S. L. Qiao, C. Yang and H. Wang, *Adv. Mater.*, 2015, **27**, 6125–6130.
- 8 (a) S. Halazy, V. Berges, A. Ehrhard and C. Danzin, *Bioorg. Chem.*, 1990, **18**, 330–344; (b) J. K. Myers and T. S. Widlanski, *Science*, 1993, **262**, 1451–1453; (c) J. R. Betley, S. Cesaro-Tadic, A. Mekhafia, J. H. Rickard, H. Denham, L. J. Partridge, A. Pluckthun and G. M. Blackburn, *Angew. Chem., Int. Ed.*, 2002, **41**, 775–777; (d) Y. T. Chang, C. M. Cheng, Y. Z. Su, W. T. Lee, J. S. Hsu, G. C. Liu, T. L. Cheng and Y. M. Wang, *Bioconjugate Chem.*, 2007, **18**, 1716–1727; (e) L. M. Chauvigne-Hines, L. N. Anderson, H. M. Weaver, J. N. Brown, P. K. Koech, C. D. Nicora, B. A. Hofstad, R. D. Smith, M. J. Wilkins, S. J. Callister and A. T. Wright, *J. Am. Chem. Soc.*, 2012, **134**, 20521–20532; (f) S. Gnaim and D. Shabat, *Acc. Chem. Res.*, 2014, **47**, 2970–2984.
- 9 (a) T. C. Cheng, S. R. Roffler, S. C. Tzou, K. H. Chuang, Y. C. Su, C. H. Chuang, C. H. Kao, C. S. Chen, I. H. Harn, K. Y. Liu, T. L. Cheng and Y. L. Leu, *J. Am. Chem. Soc.*, 2012, **134**, 3103–3110; (b) H. Song, Y. Li, Y. Chen, C. Xue and H. Xie, *Chem.–Eur. J.*, 2019, **25**, 13994–14002.
- 10 D. H. Kwan, H. M. Chen, K. Ratananikom, S. M. Hancock, Y. Watanabe, P. T. Kongsaree, A. L. Samuels and S. G. Withers, *Angew. Chem., Int. Ed.*, 2011, **50**, 300–303.
- 11 (a) J. Y. Ge, L. Li and S. Q. Yao, *Chem. Commun.*, 2011, **47**, 10939–10941; (b) C. H. Tai, C. P. Lu, S. H. Wu and L. C. Lo, *Chem. Commun.*, 2014, **50**, 6116–6119; (c) T. Doura, M. Kamiya, F. Obata, Y. Yamaguchi, T. Y. Hiyama, T. Matsuda, A. Fukamizu, M. Noda, M. Miura and Y. Urano, *Angew. Chem., Int. Ed.*, 2016, **55**, 9620–9624; (d) W. Mao, L. Xia, Y. Wang and H. Xie, *Chem.–Asian J.*, 2016, **11**, 3493–3497; (e) Z. Z. Gao, A. J. Thompson, J. C. Paulson and S. G. Withers, *Angew. Chem., Int. Ed.*, 2018, **57**, 13538–13541; (f) H. Ito, Y. Kawamata, M. Kamiya, K. Tsuda-Sakurai, S. Tanaka, T. Ueno, T. Komatsu, K. Hanaoka, S. Okabe, M. Miura and Y. Urano, *Angew. Chem., Int. Ed. Engl.*, 2018, **57**, 15702–15706; (g) J. Y. Hyun, S. H. Park, C. W. Park, H. B. Kim, J. W. Cho and I. Shin, *Org. Lett.*, 2019, **21**, 4439–4442; (h) M. Chiba, M. Kamiya, K. Tsuda-Sakurai, Y. Fujisawa, H. Kosakamoto, R. Kojima, M. Miura and Y. Urano, *ACS Cent. Sci.*, 2019, **5**, 1676–1681; (i) J. L. Jiang, Q. W. Tan, S. X. Zhao, H. Song, L. Q. Hu and H. X. Xie, *Chem. Commun.*, 2019, **55**, 15000–15003.
- 12 (a) J. E. Coleman, *Annu. Rev. Biophys. Biomol. Struct.*, 1992, **21**, 441–483; (b) O. Maldonado, R. Demasi, Y. Maldonado, M. Taylor, F. Troncale and R. Vender, *J. Clin. Gastroenterol.*, 1998, **27**, 342–345; (c) N. K. Tonks, *Nat. Rev. Mol. Cell Biol.*, 2006, **7**, 833–846; (d) Y. Shi, *Cell*, 2009, **139**, 468–484; (e) U. Sharma, D. Pal and R. Prasad, *Indian J. Clin. Biochem.*, 2014, **29**, 269–278.
- 13 (a) H. W. Liu, X. X. Hu, L. Zhu, K. Li, Q. Rong, L. Yuan, X. B. Zhang and W. Tan, *Talanta*, 2017, **175**, 421–426; (b) Y. Tan, L. Zhang, K. H. Man, R. Peltier, G. Chen, H. Zhang, L. Zhou, F. Wang, D. Ho, S. Q. Yao, Y. Hu and H. Sun, *ACS Appl. Mater. Interfaces*, 2017, **9**, 6796–6803; (c) T. H. H. C. S. Park, M. Kim, N. Raja, H. S. Yun, M. J. Sung, O. S. Kwon, H. Yoon and C. S. Lee, *Biosens. Bioelectron.*, 2018, **105**, 151–158; (d) X. Niu, K. Ye, L. Wang, Y. Lin and D. Du, *Anal. Chim. Acta*, 2019, **1086**, 29–45; (e) Y. Han, J. Chen, Z. Li, H. Chen and H. Qiu, *Biosens. Bioelectron.*, 2020, **148**, 111811–111821.
- 14 R. Yan, Y. Hu, F. Liu, S. Wei, D. Fang, A. J. Shuhendler, H. Liu, H.-Y. Chen and D. Ye, *J. Am. Chem. Soc.*, 2019, **141**, 10331–10341.
- 15 (a) L. Yuan, W. Lin, S. Zhao, W. Gao, B. Chen, L. He and S. Zhu, *J. Am. Chem. Soc.*, 2012, **134**, 13510–13523; (b) H. Chen, B. Dong, Y. Tang and W. Lin, *Acc. Chem. Res.*, 2017, **50**, 1410–1422.
- 16 (a) X. Wu, W. Shi, X. Li and H. Ma, *Acc. Chem. Res.*, 2019, **52**, 1892–1904; (b) L. H. Li, Z. Li, W. Shi, X. H. Li and H. M. Ma, *Anal. Chem.*, 2014, **86**, 6115–6120; (c) Z. Luo, L. Feng, R. An, G. Duan, R. Yan, H. Shi, J. He, Z. Zhou, C. Ji, H. Y. Chen and D. Ye, *Chem.–Eur. J.*, 2017, **23**, 14778–14785; (d) L. Li, W. Shi, X. Wu, X. Li and H. Ma, *Anal. Bioanal. Chem.*, 2018, **410**, 6771–6777.
- 17 (a) L. Wu, Y. Wang, T. D. James, N. Jia and C. Huang, *Chem. Commun.*, 2018, **54**, 5518–5521; (b) N. Kumari, M. A. Ciuba and M. Levitus, *Methods Appl. Fluoresc.*, 2019, **8**, 015004; (c) X. Li, Y. Hu, X. Li and H. Ma, *Anal. Chem.*, 2019, **91**, 11409–11416; (d) L.-Q. Niu, J. Huang, Z.-J. Yan, Y.-H. Men, Y. Luo, X.-M. Zhou, J.-M. Wang and J.-H. Wang, *Spectrochim. Acta, Part A*, 2019, **207**, 123–131; (e) X. Li, X. Li and H. Ma, *Chem. Sci.*, 2020, **11**, 1617–1622.
- 18 C. W. Lin, M. Sasaki, M. L. Orcutt, H. Miyayama and R. M. Singer, *J. Histochem. Cytochem.*, 1976, **24**, 659–667.

